Journal of Sol-Gel Science and Technology (2019) 91:82–91
https://doi.org/10.1007/s10971-019-05009-z

ORIGINAL PAPER: SOL–GEL AND HYBRID MATERIALS FOR CATALYTIC, PHOTOELECTROCHEMICAL AND SENSOR APPLICATIONS

ZnS–CdS–TaON nanocomposites with enhanced stability and photocatalytic hydrogen evolution activity

Lin An[1] · Xin Han[1] · Yaogang Li[2] · Chengyi Hou[1] · Hongzhi Wang[1] · Qinghong Zhang[1,2]

Received: 22 October 2018 / Accepted: 26 April 2019 / Published online: 24 May 2019

Abstract

In recent years, tantalum oxynitride (TaON) semiconductor as one of the most efficient photocatalysts has been studied intensively owing to the appropriate potentials for overall solar water splitting. In this work, ZnS/CdS/γ-TaON composite photocatalysts with wide light response were successfully prepared by nitridation of Ta_2O_5 at 800 °C in a wet NH_3 flowing and subsequently deposition CdS and ZnS quantum dots. The powders were characterized by X-ray diffraction (XRD), scanning electron microscopy (SEM), transmission electron microscopy (TEM), UV–vis diffuse reflection spectroscopy (DRS), N_2 adsorption–desorption isothermals, X-ray photoelectron spectroscopy (XPS), and so on. The photocatalytic property for hydrogen production was also studied. The results indicated that CdS and ZnS quantum dots with a diameter of 3–8 nm were uniformly dispersed on the surface of γ-TaON, which enlarged the spectral response of the ZnS/CdS/γ-TaON photocatalysts. And the optimized H_2 evolution rate of ZnS/CdS/γ-TaON composite (839.6 μmol h^{-1} g^{-1}) is about 14 times higher than that of CdS/γ-TaON in the absence of any noble-metal cocatalyst and 47 times higher than that of Pt loaded γ-TaON sample. The enhanced photocatalytic activity is attributed to the higher separation efficiency of electrons and holes with the heterogeneous junction between ZnS, CdS, and γ-TaON. Besides, the presence of γ-TaON and ZnS also prevent the photocorrosion of CdS. The results provide a new insight for developing the TaON-based nanocomposite photocatalysts with enhanced stability and excellent photocatalytic H_2 production activity.

Supplementary information The online version of this article (https://doi.org/10.1007/s10971-019-05009-z) contains supplementary material, which is available to authorized users.

✉ Hongzhi Wang
wanghz@dhu.edu.cn

✉ Qinghong Zhang
zhangqh@dhu.edu.cn

[1] State Key Laboratory for Modification of Chemical Fibers and Polymer Materials, College of Materials Science and Engineering, Donghua University, 201620 Shanghai, China

[2] Engineering Research Center of Advanced Glasses Manufacturing Technology, MOE, College of Materials Science and Engineering, Donghua University, 201620 Shanghai, China

Graphical Abstract

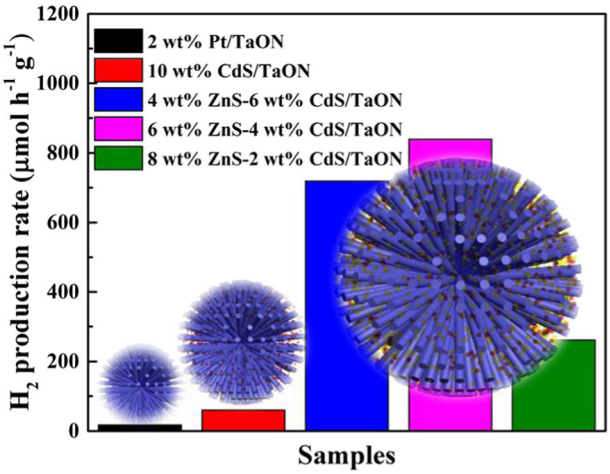

Highlights

- ZnS/CdS/γ-TaON nanocomposite photocatalysts had been successfully fabricated though deposition of CdS and ZnS quantum dots over γ-TaON nanoparticles.
- CdS and ZnS/CdS significantly improve the photocatalytic activity of γ-TaON.
- The optimized H2 evolution rate of ZnS/CdS/γ-TaON composite is about 14 times higher than that of CdS/γ-TaON in the absence of any noble metal cocatalyst and 47 times higher than that of Pt loaded γ-TaON sample.
- The band structures and the possible transfer mechanism were proposed.

Keywords ZnS · CdS · γ-TaON · Photocatalysts · Hydrogen production

1 Introduction

Since the discovery of photocatalytic splitting of water on TiO_2 electrodes in 1972 [1], photocatalytic and photoelectrochemical water splitting using solar energy has become one of the most promising methods for the production of H_2 from water and attracts a lot of attention in recent years [2, 3]. So far, numerous semiconductor photocatalysts have been studied in water splitting, such as $BiVO_4$, Cu_2O, Ta_3N_5, TaON, CdS, and g-C_3N_4 [4–9]. Among them, tantalum oxynitride (TaON) is one of the most efficient photocatalysts owing to its high dielectric and constant appropriate potentials for overall solar water splitting [10–13]. TaON contains two polymorphs β-TaON and γ-TaON. The metastable polymorph of TaON, γ-TaON which was found by Lerch et al. in 2007 [14], is proved to be more active [15]. However, pure γ-TaON is difficult to obtain, leading to few research works on the photocatalytic water splitting for hydrogen production. In addition, although TaON has suitable bandgap positions, its photocatalytic H_2 evolution activity is suppressed in practical applications. Previous studies have shown that the photocatalytic hydrogen evolution efficiency of TaON without metal cocatalysts modification was very low due to its insufficient charge transport, self-oxidative deactivation, and low-surface activity [16].

In order to enhance the photocatalysis efficiency, a great deal of work has been done including constructing various morphologies, loading cocatalysts on the surface, doping, preparing heterojunction composites with other semiconductors, and so on [17–25]. In particular, constructing the heterostructure is an effective strategy to enhance the photocatalytic efficiency, which not only can expand the light absorption range but also reduce the recombination of photogenerated electrons and holes [26]. For instance, the preparation of heterojunction composite by combining ZrO_2 and β-TaON can significantly increase the apparent quantum yield to 6.3% at 420.5 nm [16]. CdS@β-TaON core–shell composite with a platinum (Pt) cocatalyst can also increase photocatalytic activity as a result of the efficient separation of the photogenerated electron–hole pairs [27]. In addition, AgCl/Ag/γ-TaON, MoS_2/CdS/γ-TaON, $Ni(OH)_2$/TaON, and CQDs/H-γ-TaON also have been investigated and applied for enhancing its photocatalytic H_2 generation activity [28–31].

CdS, with a suitable bandgap (2.4 eV), is also one of the most concerned metal sulfide photocatalysts because of its excellent photocatalytic H_2 generation performance. Unfortunately, the inherent aggregation and photocorrosion of CdS limit its application [32, 33]. Therefore, many approaches have been proposed to improve its stability and

photocatalytic activity, such as preparing hierarchical structure to provide more active adsorption sites [34, 35] and coupling CdS with other cocatalysts or semiconductors (like MoS_2 or PdS) to enhance its activity of H_2 evolution [36, 37]. It is worth mentioned that the CdS/ZnS composite has aroused general concern because of the hole transfer and electron-tunneling mechanism [38–43].

Herein, we synthesized ZnS/CdS/γ-TaON nanocomposites through deposition of CdS and ZnS quantum dots on the surface of γ-TaON nanoparticles. The CdS and ZnS quantum dots can effectively enhance the photocatalytic hydrogen production activity and stability of ZnS/CdS/γ-TaON nanocomposites. For comparison, the CdS–ZnS photocatalyst was also synthesized in a similar way. All the composites were investigated by various characterization methods. And the results indicated that the photocatalytic H_2 generation activity of ZnS/CdS/γ-TaON nanocomposites is much higher than that of pure γ-TaON and CdS/γ-TaON. The 6 wt% ZnS/4 wt% CdS/γ-TaON composite exhibited the optimized H_2 evolution rate of 839.6 μmol h^{-1} g^{-1}. Besides, the formation process and possible transfer mechanism of charge carriers were also proposed in detail.

2 Experimental

2.1 Synthesis of γ-TaON

γ-TaON was prepared as in previous work [15]. Briefly, 1.0 g Ta powder (Aladdin, high-CV) was added into a 100 ml volume para polyphenol (PPL-lined) cylindrical autoclave, which contained 70 ml of distilled water, 1.3 ml 40 wt% hydrofluoric acid (HF, Sinopharm Chemical Reagent Co., Ltd, AR) solution and 4.0 ml 30 wt% hydrogen peroxide (H_2O_2, Sinopharm Chemical Reagent Co., Ltd, AR) solution, and the autoclave was heated in an oven at 240 °C for 12 h. The white tantalum oxide (Ta_2O_5) precipitation was washed with ethanol, deionized water, and dried at 60 °C for 12 h. Ta_2O_5 powder was then nitrided to form γ-TaON in an atmosphere of flowing wet ammonia gas (100 ml min^{-1}) at 800 °C for 5 h.

2.2 Synthesis of ZnS/CdS/γ-TaON, CdS, and ZnS/CdS nanocomposites

The ZnS/CdS/γ-TaON nanocomposites were prepared by modified sol–gel method. And the precursor solution of CdS and ZnS quantum dots were prepared by sol–gel methods, using $Cd(NO_3)_2{\cdot}4H_2O$, $Zn(CH_3COO)_2{\cdot}2H_2O$, and C_2H_5NS as the raw materials and PVP-K30 as the complexing agent. In order to accelerate the reaction rate, ammonia water was added into the solution. Depending on different content of ZnS and CdS, the ZnS/CdS/γ-TaON composite photocatalysts were denoted as nZ-CT, where "*n*" represented 0, 4, 6, and 8 wt% of the amount of ZnS nanocrystals (0Z-CT, 4Z-CT 6Z-CT, and 8Z-CT). The total content of ZnS and CdS in the ZnS/CdS/γ-TaON composites is 10 wt%, and that of γ-TaON is 90 wt% through all experiments. The content of γ-TaON, CdS, and ZnS in different Z-CT samples is shown in Table 1.

Taking 6Z-CT as an example, the preparation process was as follows: as-synthesized γ-TaON (0.45 g) and thioacetamide (TAA, Sinopharm Chemical Reagent Co., Ltd, AR, 0.3353 g) were added into 25 ml of the ethyl alcohol (EtOH)/H_2O mixed solvent (2:3, v/v) and stirred for 60 min (Suspension A). Cadmium nitrate tetrahydrate ($Cd(NO_3)_2{\cdot}4H_2O$, Aladdin, metals basis, 0.5338 g) and polyvinyl pyrrolidone K30 (PVP-K30, Sinopharm Chemical Reagent Co., Ltd, GR, 1 g) were dissolved into 25 ml EtOH/H_2O mixed solvent (2:3, v/v) and stirred into a clear solution (Solution B). Similarly, zinc acetate ($Zn(CH_3COO)_2{\cdot}2H_2O$, Aladdin, metals basis, 0.5632 g) and PVP-K30 (1 g) were dissolved into 25 ml EtOH/H_2O mixed solvent (2:3, v/v) and stirred into a clear solution (Solution C). Subsequently, added 1 ml ammonium hydroxide aqueous solution ($NH_3{\cdot}H_2O$, Sinopharm Chemical Reagent Co., Ltd, AR) and 2 ml Solution B into Suspension A kept in an oil bath at 100 °C for 2 h under continuously stirring. Kept at the same temperature, continue to add 1 ml $NH_3{\cdot}H_2O$ and 3 ml Solution C stirring for further 2 h and then naturally cooled to room temperature. The precipitates were washed with DI

Table 1 γ-TaON, CdS, and ZnS content of the Z-CT samples

Samples	γ-TaON content in the composite (wt%)	CdS content in the composite (wt%)	ZnS content in the composite (wt%)
0Z-CT	90	10	0
4Z-CT	90	6	4
6Z-CT	90	4	6
8Z-CT	90	2	8

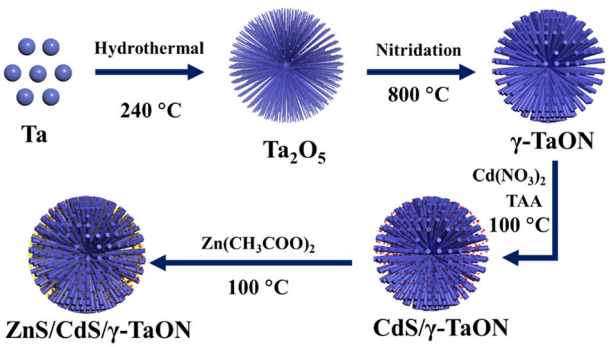

Scheme 1 Schematic illustration of the formation process of Z-CT samples

water and absolute ethanol for several times and dried in a vacuum oven at 60 °C for 12 h to obtain the final composite powders. 0Z-CT, 4Z-CT, and 8Z-CT were fabricated by changing the addition of Solution B and Solution C. The preparation methods of CdS and CdS-ZnS catalysts were similar to the Z-CT in absence of γ-TaON, which are named as CdS and 4CdS-6ZnS. The formation process of Z-CT samples is illustrated in Scheme 1. First of all, Ta powder was oxidized to Ta_2O_5 with dandelion-like structure and then transformed to TaON with a similar structure. After that, CdS and ZnS quantum dots were loaded on the γ-TaON surface to improve its photocatalytic efficiency.

2.3 Characterization

X-ray diffraction (XRD) was carried out on a Rigaku-D/max 2550 PC (Japan) diffractometer with Cu Kα radiation ($\lambda = 1.5406$ Å), at a scan rate of 10°/min. The morphology of the samples was characterized with a field emission scanning electron microscope (FESEM, Hitachi S-4800) operated at an accelerating voltage of 20 kV. Transmission electron microscopy (TEM) and STEM images were obtained using an FEI Talos F200S instrument operating at 200 kV. UV–vis diffuse reflectance spectroscopy (DRS) spectra were recorded on a Shimadzu UV-3600 instrument, using $BaSO_4$ as the reference sample, in the range 200–800 nm. The nitrogen adsorption–desorption isotherms of samples were measured using an automatic volumetric sorption analyzer (Autosorb-1 MP, Quantachrome Instruments, USA) at liquid-nitrogen temperature 77 K. Prior to the N_2 adsorption–desorption measurement, all samples were degassed at 200 °C under vacuum for 5 h to remove impurities. X-ray photoelectron spectroscopy (XPS) valence band (VB) spectra were performed on a photoelectron spectrometer (Escalab 250Xi, Thermo Fisher Scientific Inc., USA).

2.4 Photocatalytic tests

Photocatalytic hydrogen evolution experiments were carried out in a quartz reaction vessel connected to a glass-closed gas circulation system (Labsolar-IIIAG, PerfectLight, China). Hundred milligrams of the Z-CT sample was dispersed under constant stirring in a 100 ml mixed aqueous solution containing 0.35 M Na_2S and 0.25 M Na_2SO_3. For comparison, pure γ-TaON decorated with Pt photocatalyst was also prepared through photoreduction by dissolving a certain amount of H_2PtCl_6 in the solution (named as Pt/T). The reactant solution with gas circulation system was evacuated several times to remove air completely. Then the solution was irradiated using 300 W xenon lamp with an AM 1.5 filter (the transmission spectrum of the filter as shown in Fig. S1) or cutoff filter of 420 nm. The evolved gas was detected by gas chromatography (GC7900, Techcomp, China).

2.5 Photoelectrochemical measurements

Photocurrent experiments were implemented using a VSP-300 (Bio-Logic, France) electrochemical workstation in the applied potential of 0.9 V versus Ag/AgCl (saturated KCl). The electrochemical cell was consisted of a standard three-electrode, with a Pt foil as a counter electrode, an Ag/AgCl as a reference electrode, the photocatalyst coated on a fluorine-doped tin oxide (FTO)-conductive glass as the working electrode and a sodium sulfate aqueous solution (Na_2SO_4, 0.5 M) as an electrolyte. The working electrodes were prepared by dropping method described in our previous work in detail [44]. Typically, the as-prepared γ-TaON, 0Z-CT or 6Z-CT powder (4 mg), EtOH/H_2O mixed solvent (1:4, v/v, 1 ml), and Nafion solution (5 wt%, 10 µl) were mixed to get a slurry. The slurry (80 µl) was then spread onto a pre-cleaned FTO plate (an active area of 1 cm^2) surface using a pipette, and the working electrodes were dried at room temperature for 12 h before use. A 300 W xenon lamp with AM 1.5 filter was used as the light source.

3 Results and discussion

The phase of Ta_2O_5 was characterized by XRD as shown in Fig. S2. The pattern shows only two diffraction peaks at 22.8° and 46.3°, which correspond to the (001) and (002) faces of orthorhombic Ta_2O_5 (JCPDS 71–0639), respectively. The stronger (001) peak suggests that the Ta_2O_5 was preferentially growing along (001) direction. Figure S3 shows the XRD pattern of 4CdS-6ZnS sample, and the result reveals that the photocatalyst was composed of CdS (JCPDS 75–1546) and ZnS (JCPDS 80–0020) species. Furthermore, the γ-TaON and Z-CT samples were characterized using XRD as shown in Fig. 1. The major peaks of metastable γ-TaON powder are located at 2θ equal to 13.8°, 22.9°, 23.9°, 27.8°, 31.7°, 37.8°, and 46.8°, respectively, which is consistent with its code ICSD#173006 [15]. No peaks attributed to Ta_2O_5, β-TaON, or Ta_3N_5 were observed, implying that the pure phase of γ-TaON was obtained. All diffraction peaks of the ZnS/CdS/γ-TaON composites are well indexed according to γ-TaON phase, and no characteristic diffraction peaks for CdS and ZnS species are observed, which should be ascribed to the less amount and small size of ZnS/CdS particles. Moreover, there is no obvious shift of the peak positions in each of the materials, suggesting that ZnS/CdS only deposited on the surface of TaON rather than incorporating into its lattice, which are in agreement with the previous reports [29, 30].

Figure 2 shows the morphology of Ta_2O_5 and γ-TaON. The scanning electron microscopy (SEM) image of Ta_2O_5 (Fig. 2a) shows that the self-assembly of Ta_2O_5 is chrysanthemum-like hierarchical nanostructures consisting of nanorods with a diameter of 10–20 nm and a length of 200–300 nm. The HRTEM image of Ta_2O_5 (Fig. 2c) shows an interplanar spacing of 0.388 nm, which can be assigned to the (001) plane of orthorhombic phase Ta_2O_5, which is in accord with the XRD results. Figure 2b, d shows the morphology of γ-TaON. Compared with Ta_2O_5, event though the structure of the γ-TaON had not been a major changed, the diameter of nanorods was increase to 20–30 nm and the length of nanorods was shortened to 100–200 nm after high temperature nitriding treatment.

Figure 3a–c shows the morphology of 6Z-CT sample. There is also no significant difference between γ-TaON and 6Z-CT except that some ultrafine nanocrystals are attached to the surface of nanorods (Fig. 3a, c). The HRTEM image (Fig. 3b) of 6Z-CT sample shows that the particles consist of many quantum dots with a diameter of 3–8 nm and well dispersed on the surface of γ-TaON. The image shows the interplanar spacings of 0.338 nm and 0.308 nm, which are consistent with the distance of (111) planes of CdS and (111) planes of ZnS. The EDX spectrum (Fig. 3d) shows that the 6Z-CT sample consists of Ta, O, N, Zn, Cd, S, and Pt elements, while the signal of Pt came from the substrate in order to improve electrical conductivity for EDS analysis. In addition, the STEM–EDX elemental mapping (Fig. S4) is in good agreement with the EDS result. Above results indicate that the CdS and ZnS nanoparticals are uniformly dispersed on the surface of γ-TaON.

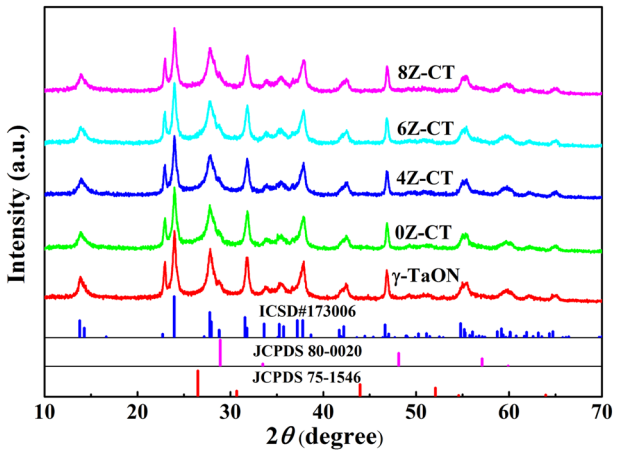

Fig. 1 XRD patterns of γ-TaON and Z-CT samples

The optical properties of Ta_2O_5, γ-TaON, and Z-CT materials were measured by UV–vis DRS in the wavelength range of 200–800 nm. As shown in Fig. 4, with the decrease of CdS content (0Z-CT > 4Z-CT > 6Z-CT > 8Z-CT), the light absorption in 450–470 nm of the samples significantly decreases, and the absorption edges exhibit a blue shift, due to the wide bandgap of ZnS. The corresponding bandgap energies of Ta_2O_5, γ-TaON, and 0Z-CT samples could be estimated through the Kubelka–Munk method (Fig. 4 inset), which is about 3.93, 2.71, and 2.49 eV, respectively.

Figure 5 shows the N_2 adsorption–desorption isotherms of Ta_2O_5, γ-TaON, and Z-CT particles. The BET surface area reduces remarkably from 85.4 m^2/g for Ta_2O_5 to 14.1 m^2/g for γ-TaON due to the high-temperature nitridation reaction. The SEM and HRTEM images (Fig. 3) also indicated that γ-TaON particles had shorter and thicker nanorods than Ta_2O_5. The BET surface areas of 0Z-CT and 6Z-CT increases to 18.2 and 20.1 m^2/g, which could be attributed to the introduction of CdS and ZnS quantum dots.

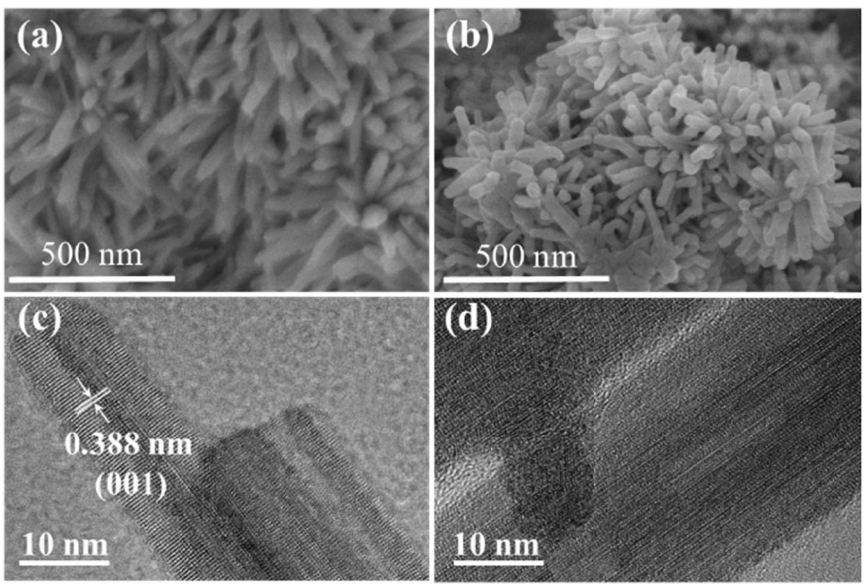

Fig. 2 SEM and HRTEM images of Ta_2O_5 (**a**, **c**) and γ-TaON (**b**, **d**) samples

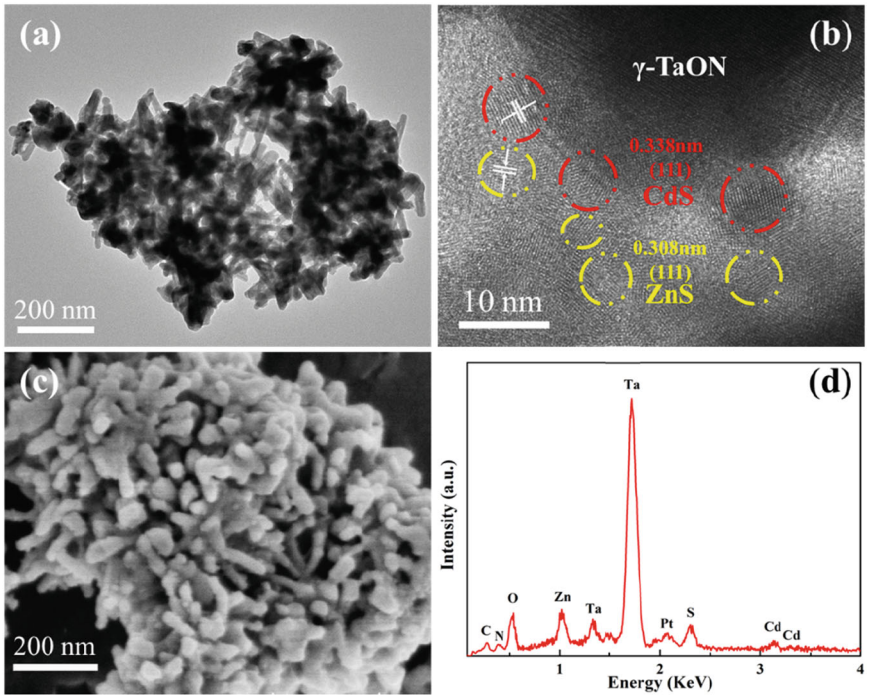

Fig. 3 TEM (**a**), HRTEM (**b**), SEM (**c**) images and EDS spectra (**d**) of 6Z-CT sample

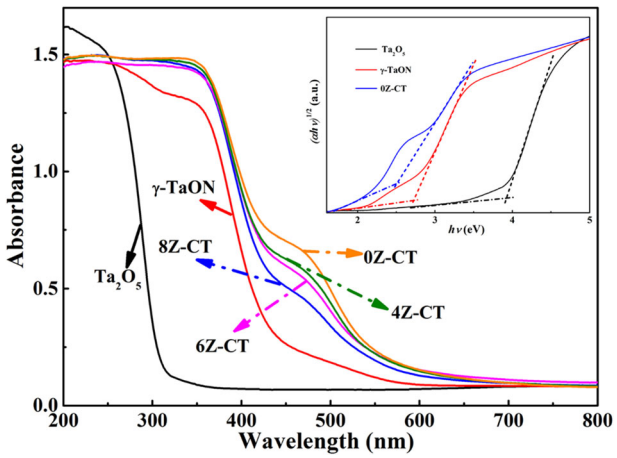

Fig. 4 UV–vis diffuse reflectance spectra and hν versus $(\alpha h\nu)^{1/2}$ graph (**inset**) of the as-prepared samples

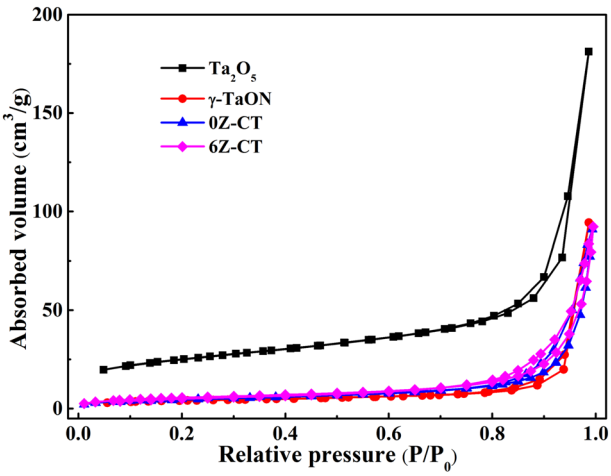

Fig. 5 N_2 adsorption–desorption isotherms of Ta_2O_5, γ-TaON, 0Z-CT, and 6Z-CT samples

The larger specific surface area indicates that the Z-CT samples can offer more available reaction active sites for photocatalystic process.

The XPS of the samples was further measured and used to study the chemical composition and surface electron state of elements in CdS, Z-CT, and 4CdS-6ZnS samples. Figure 6 displays the full XPS spectrum and high-resolution spectra of the 6Z-CT sample. The XPS survey spectrum in Fig. 6a shows the presence of Ta, O, N, Cd, Zn, and S elements, which is consistent with the result of its EDX (Fig. 3d) and STEM–EDX (Fig. S4). Figure S5 shows the comparison of high-resolution spectra in CdS, 4CdS-6ZnS, and 6Z-CT samples. As can be seen from Fig. S5a, the two peaks at 404.5 eV and 411.2 eV are assigned to Cd $3d_{5/2}$ and Cd $3d_{3/2}$ for CdS sample, showing good agreement with literature data [45, 46]. In comparison with the pure CdS, the typical peaks of Cd 3d for the 4CdS-6ZnS and 6Z-CT samples shifted to lower energies of 404.1 eV and 410.9 eV. The lowered binding energy is because of the interaction between CdS and ZnS. Previous XPS studies of CdS also observed a lower binding energy component [47, 48]. There are no obvious changes of the binding energy of Zn 2p. The high-resolution XPS spectrum of Zn 2p shows two peaks at 1021.0 eV and 1044.0 eV, which correspond to Zn $2p_{1/2}$ and Zn $2p_{3/2}$ in ZnS (Figs 6c and S5b) [49, 50]. The peaks of S $2p_{3/2}$ (160.7 eV) and S $2p_{1/2}$ (161.8 eV) at Fig. 6d

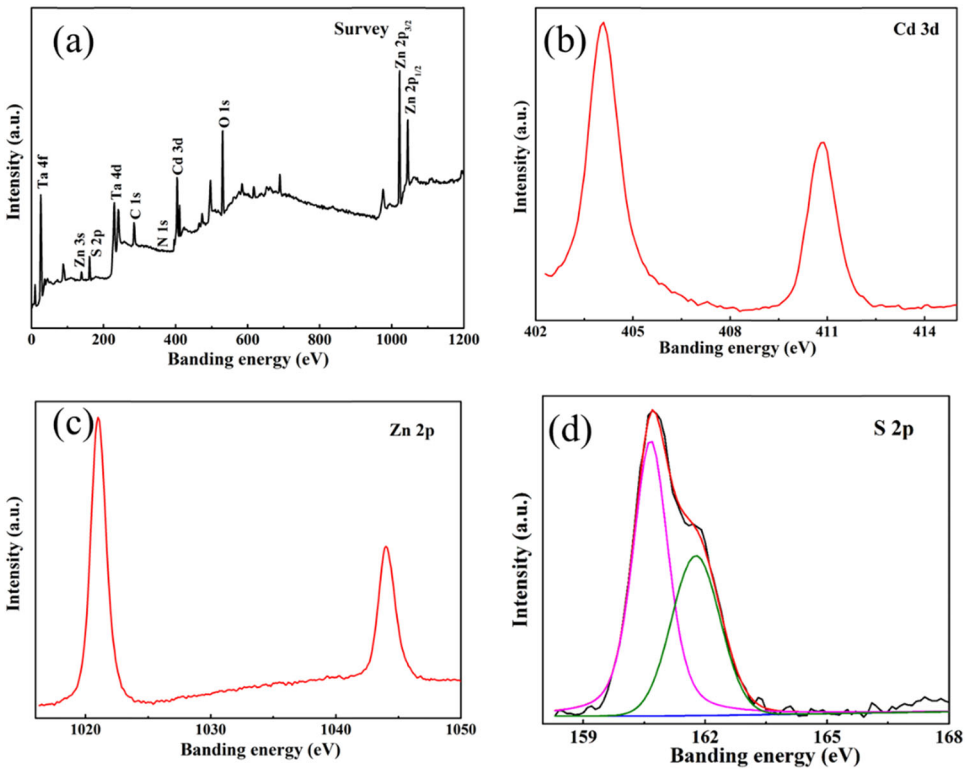

Fig. 6 XPS survey spectrum (**a**) and high-resolution spectra of **b** Cd 3d, **c** Zn 2p, **d** S 2p of 6Z-CT sample

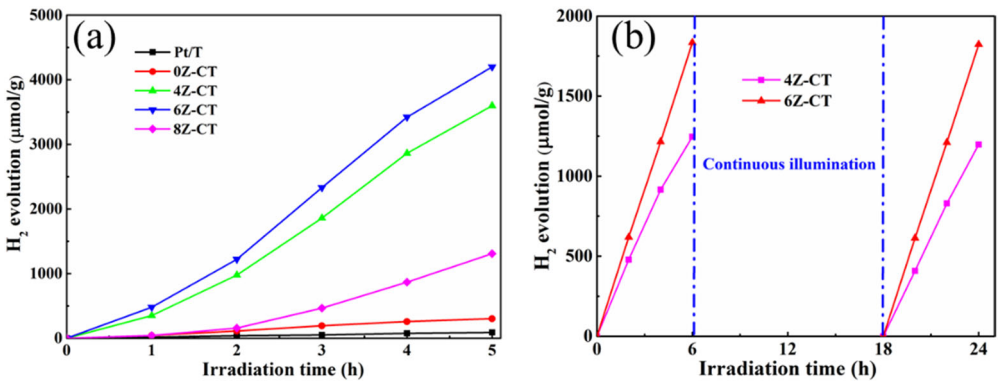

Fig. 7 Hydrogen production rates (**a**) of as-prepared samples and long-term photocatalytic H_2 production (**b**) of the Z-CT photocatalysts after storage in natural ambient environment for 24 months

demonstrate the existence of S^{2-}. All the results indicate the formation of both ZnS and CdS.

Photocatalytic H_2 production activities of the Z-CT composites with different contents of ZnS/CdS were investigated under irradiation using Na_2S–Na_2SO_3 as sacrificial agents without loading any noble metal cocatalyst, as shown in Fig. 7. A 2 wt% Pt-loaded TaON sample (Pt/T) was also tested as the control group under the same experimental condition (catalyst, 100 mg; reactant solution, 100 ml mixed aqueous solution containing 0.35 M Na_2S and 0.25 M Na_2SO_3; light source, xenon lamp (300 W) with an AM 1.5 filter; reaction vessel, top-irradiation type). In Fig. 7a, it is shown that after illumination for 5 h, the Pt/T sample shows relatively low-photocatalytic activity (18 μmol h^{-1} g^{-1}) comparing with Z-CT samples, which may be due to the rapid recombination of photon-generated carriers in composites and the large overpotential for hydrogen production. It is noteworthy that only pure CdS loaded sample (0Z-CT) shows obviously improved photocatalytic H_2 evolution activity (60 μmol h^{-1} g^{-1}), which is almost 3.3 times higher than that of the Pt/T sample. In addition, with increasing ZnS content, the Z-CT photocatalysts exhibit higher photocatalytic activity. 6Z-CT sample exhibits the highest photocatalytic activity with the H_2 evolution rate of 839.6 μmol h^{-1} g^{-1}, which is about 14 times higher than that of 0Z-CT and 47 times higher than that of the Pt/T sample. The present ZnS/CdS/γ-TaON system

has higher H_2 evolution rate than other TaON-based systems, such as TaON/Bi_2O_3 and TaON/$Ni(OH)_2$ [30, 51]. However, further increases in the ZnS content leads to a gradual decrease of the photocatalytic activity. It is most likely that the increase amount of ZnS decreased the active sites for H_2 evolution on the γ-TaON surface. Similar study has also been reported in the ZnS/CdS system [39]. Compared with Z-CT, Pt-loaded TaON catalyst shows a lower activity which means the heterostructure of Z-CT plays an important role in enhancing the photocatalytic activity promoting the separation of photogenerated electron and hole pairs. As shown in Fig. S6, the photocatalytic H_2 production activity of the 6Z-CT composite was also evaluated under visible light irradiation ($\lambda > 420$ nm), by using 0.35 M Na_2S and 0.25 M Na_2SO_3 aqueous solution as sacrificial agent, where the average hydrogen generation rate of the 6Z-CT sample is 163 μmol h^{-1} g^{-1}. Furthermore, the 6Z-CT photocatalyst exhibited a stable photocatalytic activity even after 9 h without renewing the sacrificial agent, suggesting its good stability for H_2 production. Overall, ZnS and CdS play a vital role in photocatalytic H_2 production activity.

More importantly, the catalytic activity of the samples was evaluated after storing 2 years under natural ambient environment, it was found that no obvious activity decrease was observed after 24 h continuous illumination (Fig. 7b), which indicates the excellent stability of Z-CT samples. The hydrogen evolution rate of 4Z-CT and 6Z-CT sample decreases to 207.6 and 305.7 μmol h^{-1} g^{-1}, which may be resulted from the instability of CdS. For comparison, Figures S7 and S8 show the long-term photocatalytic H_2 production activity of freshly prepared CdS and 4CdS-6ZnS samples under the same conditions. The hydrogen evolution rate of fresh pure CdS sample decreases from 24.5 to 11.8 μmol h^{-1} g^{-1}. A rapid decline of H_2 production rate is also detected when 4CdS-6ZnS sample working as the photocatalyst, which is shown in Fig. S8. All the results revealed that the heterostructure of ZnS/CdS/γ-TaON plays an important role in improving the working stability. The photocorrosion of CdS can be significantly reduced by coupling of γ-TaON and ZnS. All the results demonstrate that the heterogeneous junction between ZnS, CdS, and γ-TaON can effectively promote the separation of photogenerated electrons and holes.

The transient photocurrent responses of the γ-TaON, 0Z-CT, and 6Z-CT electrodes were also tested to research the behavior of photogenerated electron–hole pairs with eight on–off cycles of intermittent illumination. As shown in Fig. 8, the three electrodes exhibit sensitive photocurrent responses and similar shapes of photocurrent curves. The electrodes present a low dark current, while when the light is switched on, the photocurrent rapidly increases to a constant value for all samples. And the transient photocurrents of 0Z-CT and 6Z-CT samples with heterostructures

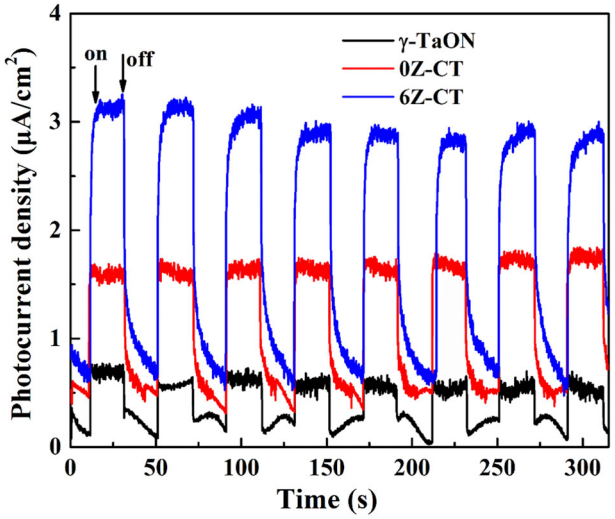

Fig. 8 Transient photocurrent responses of γ-TaON, 0Z-CT, and 6Z-CT electrodes in 0.5 M Na_2SO_4 aqueous solution under chopped 300 W xenon lamp light irradiation at 0.9 V versus Ag/AgCl

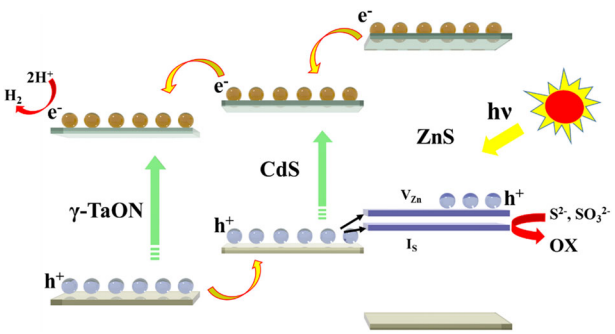

Fig. 9 Schematic illustration of photocatalytic mechanism of Z-CT samples

exhibit much higher values than that of γ-TaON attribute to their efficient separation of carriers, which is consistent with their photocatalytic H_2 production activities. Furthermore, no apparent photocurrent decrease was observed during the eight on–off cycles, which revealed that the photocatalysts have good stability.

Figure 9 shows the band structures and the possible transfer mechanism of charge carriers of the ZnS/CdS/γ-TaON system. There have been a number of studies showed that ZnS crystal has many intrinsic defects, like interstitial sulfur (I_S) and zinc vacancies (V_{Zn}) [38–40], as well as the vacancies localized above the VB of both ZnS and CdS [52]. Under irradiation, the photogenerated electrons are excited from the VB to the conduction band (CB) of ZnS, CdS, and γ-TaON, creating positive holes in the VB. Then the photo-excited electrons can transfer from ZnS and CdS to γ-TaON to generate hydrogen, while the holes migrate to CdS. Furthermore, V_{Zn} and I_s can act as acceptors for holes in CdS, as a result of effective transformation of electron–hole pairs. Moreover, the presence of both

γ-TaON and ZnS can prevent CdS from photocorrosion, thus facilitating the improvement of stability.

4 Conclusion

In summary, the ZnS/CdS/γ-TaON nanocomposite photocatalysts were synthesized by loading ZnS/CdS quantum dots on the surfaces of γ-TaON via a two-step solution-phase method. The CdS and ZnS/CdS significantly improve the photocatalytic activity for hydrogen production of γ-TaON, and the optimal content of ZnS was 6 wt%. The corresponding H_2 production rate was 839.6 μmol h^{-1} g^{-1} which was 14 times higher than that of CdS loaded alone under the same reaction conditions. This high photocatalytic H_2 production activity is mainly ascribed to the ZnS/CdS heterostructures, which can promote the charge transfer and suppress the photoelectron–hole recombination. This work shows that the oxynitrides photocatalysts have a relatively high-hydrogen production activity when it combines with also visible light-responded CdS, even without the noble metal cocatalysts. The investigation offers new facilities for TaON-based photocatalysts to make use of more visible light.

Acknowledgements We gratefully acknowledge the financial support by Natural Science Foundation of China (No.51572046, 51603037), the Shanghai Natural Science Foundation (15ZR1401200), the Program for Professor of Special Appointment (Eastern Scholar) at Shanghai Institutions of Higher Learning, Program of Shanghai Academic Research Leader (16XD1400100), Science and Technology Commission of Shanghai Municipality (16JC1400700), Innovation Program of Shanghai Municipal Education Commission (2017-01-07-00-03-E00055), and the Program of Introducing Talents of Discipline to Universities (No.111-2-04).

Compliance with ethical standards

Conflict of interest The authors declare that they have no conflict of interest.

References

1. Fujishima A, Honda K (1972) Electrochemical photolysis of water at a semiconductor electrode. Nature 238:37–38
2. Kudo A, Miseki Y (2009) Heterogeneous photocatalyst materials for water splitting. Chem Soc Rev 38:253–278
3. Hisatomi T, Kubota J, Domen K (2014) Recent advances in semiconductors for photocatalytic and photoelectrochemical water splitting. Chem Soc Rev 43:7520–7535
4. Kim TW, Choi K-S (2014) Nanoporous $BiVO_4$ photoanodes with dual-layer oxygen evolution catalysts for solar water splitting. Science 343:990–994
5. Nian J-N, Hu C-C, Teng H (2008) Electrodeposited p-type Cu_2O for H_2 evolution from photoelectrolysis of water under visible light illumination. Int J Hydrog Energy 33:2897–2903
6. Li Y, Takata T, Cha D et al. (2013) Vertically aligned Ta_3N_5 nanorod arrays for solar-driven photoelectrochemical water splitting. Adv Mater 25:125–131
7. Higashi M, Domen K, Abe R (2011) Fabrication of efficient TaON and Ta_3N_5 photoanodes for water splitting under visible light irradiation. Energy Environ Sci 4:4138–4147
8. Bao N, Shen L, Takata T, Domen K (2008) Self-templated synthesis of nanoporous CdS nanostructures for highly efficient photocatalytic hydrogen production under visible light. Chem Mater 20:110–117
9. Liu J, Liu Y, Liu N et al. (2015) Metal-free efficient photocatalyst for stable visible water splitting via a two-electron pathway. Science 347:970–974
10. Hitoki G, Takata T, Kondo JN et al. (2002) An oxynitride, TaON, as an efficient water oxidation photocatalyst under visible light irradiation (λ ≤ 500 nm). Chem Commun 1698–1699
11. Chun W-J, Ishikawa A, Fujisawa H et al. (2003) Conduction and valence band positions of Ta_2O_5, TaON, and Ta_3N_5 by UPS and electrochemical methods. J Phys Chem B 107:1798–1803
12. Hara M, Nunoshige J, Takata T et al. (2003) Unusual enhancement of H_2 evolution by Ru on TaON photocatalyst under visible light irradiation. Chem Commun 3000–3001
13. Li P, Fan W, Li Y et al. (2010) First-principles study of the electronic, optical properties and lattice dynamics of tantalum oxynitride. Inorg Chem 49:6917–6924
14. Schilling H, Stork A, Irran E et al. (2007) γ-TaON: a metastable polymorph of tantalum oxynitride. Angew Chem Int Ed 46:2931–2934
15. Wang Z, Hou J, Yang C et al. (2013) Hierarchical metastable γ-TaON hollow structures for efficient visible-light water splitting. Energy Environ Sci 6:2134–2144
16. Maeda K, Higashi M, Lu D et al. (2010) Efficient nonsacrificial water splitting through two-step photoexcitation by visible light using a modified oxynitride as a hydrogen evolution photocatalyst. J Am Chem Soc 132:5858–5868
17. Yu J, Yu Y, Zhou P et al. (2014) Morphology-dependent photocatalytic H_2-production activity of CdS. Appl Catal B 156–157:184–191
18. Thirugnanam N, Govindarajan D, Dinesh S et al. (2017) Synthesis, structural, optical and morphological properties of CdSe:Zn/CdS core–shell nanoparticles. J Sol-Gel Sci Technol 82:109–118
19. Yang J, Wang D, Han H, Li C (2013) Roles of Cocatalysts in Photocatalysis and Photoelectrocatalysis. Acc Chem Res 46:1900–1909
20. Qi L, Li X (2014) N-doped $NaTaO_3$: novel visible-light-driven photocatalysts synthesised by a sol–gel method. J Sol-Gel Sci Technol 69:625–629
21. Zhou M, Yu J, Cheng B (2006) Effects of Fe-doping on the photocatalytic activity of mesoporous TiO_2 powders prepared by an ultrasonic method. J Hazard Mater 137:1838–1847
22. Marschall R (2014) Semiconductor composites: strategies for enhancing charge carrier separation to improve photocatalytic activity. Adv Funct Mater 24:2421–2440
23. Pan H (2016) Principles on design and fabrication of nanomaterials as photocatalysts for water-splitting. Renew Sustain Energy Rev 57:584–601
24. Guo Y, Cui X, Li Y et al. (2016) The effect of aging time on the properties of Mg–Al–CO_3 layered double hydroxides and its application as a catalyst support for TiO_2. J Nanosci Nanotechnol 16:5653–5661
25. Han X, AnL, Xu D et al. (2018) Mesoporous Pt/$TiO_{2-x}N_x$ nanoparticles with less than 10 nm and high specific surface area as visible light hydrogen evolution photocatalysts. J Sol-Gel Sci Technol 87:230–239
26. Wang H, Zhang L, Chen Z et al. (2014) Semiconductor heterojunction photocatalysts: design, construction, and photocatalytic performances. Chem Soc Rev 43:5234–5244

27. Hou J, Wang Z, Kan W et al. (2012) Efficient visible-light-driven photocatalytic hydrogen production using CdS@TaON core–shell composites coupled with graphene oxide nanosheets. J Mater Chem 22:7291–7299
28. Hou J, Yang C, Wang Z et al. (2013) Three-dimensional Z-scheme AgCl/Ag/γ-TaON heterostructural hollow spheres for enhanced visible-light photocatalytic performance. Appl Catal B 142–143:579–589
29. Wang Z, Hou J, Yang C et al. (2014) Three-dimensional MoS_2–CdS–γ-TaON hollow composites for enhanced visible-light-driven hydrogen evolution. Chem Commun 50:1731–1734
30. Chen W, Chu M, Gao L et al. (2015) $Ni(OH)_2$ loaded on TaON for enhancing photocatalytic water splitting activity under visible light irradiation. Appl Surf Sci 324:432–437
31. Hou J, Cheng H, Yang C et al. (2015) Hierarchical carbon quantum dots/hydrogenated-γ-TaON heterojunctions for broad spectrum photocatalytic performance. Nano Energy 18:143–153
32. Matsumura M, Furukawa S, Saho Y, Tsubomura H (1985) Cadmium sulfide photocatalyzed hydrogen production from aqueous solutions of sulfite: effect of crystal structure and preparation method of the catalyst. J Phys Chem 89:1327–1329
33. Reber JF, Rusek M (1986) Photochemical hydrogen production with platinized suspensions of cadmium sulfide and cadmium zinc sulfide modified by silver sulfide. J Phys Chem 90:824–834
34. Xiang Q, Cheng B, Yu J (2013) Hierarchical porous CdS nanosheet-assembled flowers with enhanced visible-light photocatalytic H_2-production performance. Appl Catal B 138–139:299–303
35. Liu Y, Liu S, Wu T et al. (2017) Facile preparation of flower-like Bi_2WO_6/CdS heterostructured photocatalyst with enhanced visible-light-driven photocatalytic activity for Cr(VI) reduction. J Sol-Gel Sci Technol 83:315–323
36. Zong X, Yan H, Wu G et al. (2008) Enhancement of photocatalytic H_2 evolution on CdS by loading MoS_2 as cocatalyst under visible light irradiation. J Am Chem Soc 130:7176–7177
37. Yan H, Yang J, Ma G et al. (2009) Visible-light-driven hydrogen production with extremely high quantum efficiency on Pt–PdS/CdS photocatalyst. J Catal 266:165–168
38. Peng Xie Y, Bao YuZ, Liu G et al. (2014) CdS–mesoporous ZnS core–shell particles for efficient and stable photocatalytic hydrogen evolution under visible light. Energy Environ Sci 7:1895–1901
39. Jiang D, Sun Z, Jia H et al. (2015) A cocatalyst-free CdS nanorod/ZnS nanoparticle composite for high-performance visible-light-driven hydrogen production from water. J Mater Chem A 4:675–683
40. Kai S, Xi B, Liu X et al. (2018) An innovative Au-CdS/ZnS-RGO architecture for efficient photocatalytic hydrogen evolution. J Mater Chem A 6:2895–2899
41. Antoniadou M, Daskalaki VM, Balis N et al. (2011) Photocatalysis and photoelectrocatalysis using (CdS-ZnS)/TiO_2 combined photocatalysts. Appl Catal B 107:188–196
42. Xu X, Hu L, Gao N et al. (2015) Controlled growth from ZnS nanoparticles to ZnS–CdS nanoparticle hybrids with enhanced photoactivity. Adv Funct Mater 25:445–454
43. Xin Z, Li L, Zhang W et al. (2018) Synthesis of ZnS@CdS–Te composites with p–n heterostructures for enhanced photocatalytic hydrogen production by microwave-assisted hydrothermal method. Mol Catal 447:1–12
44. Han X, Xu D, An L et al. (2018) WO_3/g-C_3N_4 two-dimensional composites for visible-light driven photocatalytic hydrogen production. Int J Hydrog Energy 43:4845–4855
45. Tu W, Wang W, Lei J et al. (2012) Chemiluminescence excited photoelectrochemistry using graphene – quantum dots nanocomposite for biosensing. Chem Commun 48:6535–6537
46. Zhou Y, Wang Y, Wen T et al. (2016) Mesoporous $Cd_{1-x}Zn_xS$ microspheres with tunable bandgap and high specific surface areas for enhanced visible-light-driven hydrogen generation. J Colloid Interface Sci 467:97–104
47. Wakerley DW, Kuehnel MF, Orchard KL et al. (2017) Solar-driven reforming of lignocellulose to H_2 with a CdS/CdO_x photocatalyst. Nat Energy 2:17021
48. Pirkarami A, Rasouli S, Ghasemi E (2019) 3-D CdS@NiCo layered double hydroxide core-shell photoelectrocatalyst used for efficient overall water splitting. Appl Catal B 241:28–40
49. Xu M, Zai J, Yuan Y, Qian X (2012) Band gap-tunable $(CuIn)_xZn_{2(1-x)}S_2$ solid solutions: preparation and efficient photocatalytic hydrogen production from water under visible light without noble metals. J Mater Chem 22:23929–23934
50. Yoo PS, Amaranatha Reddy D, Jia Y et al. (2017) Magnetic core-shell $ZnFe_2O_4$/ZnS nanocomposites for photocatalytic application under visible light. J Colloid Interface Sci 486:136–143
51. Adhikari SP, Hood ZD, More KL et al. (2015) Visible light assisted photocatalytic hydrogen generation by Ta_2O_5/Bi_2O_3, TaON/Bi_2O_3, and Ta_3N_5/Bi_2O_3 composites. RSC Adv 5:54998–55005
52. Denzler D, Olschewski M, Sattler K (1998) Luminescence studies of localized gap states in colloidal ZnS nanocrystals. J Appl Phys 84:2841–2845